RSC Advances

PAPER

View Article Online
View Journal | View Issue

Cite this: *RSC Adv.*, 2022, **12**, 32027

Theoretical study on the ferroelectric and light absorption properties of Li_2SbBiO_6 for harvesting visible light

Xing-Yuan Chen, *[a] Shi-Wu Ling,[a] Hua-Kai Xu,[a] You-Da Che,[a] Li-Fang Chen,[a] Xiang-Fu Xu,[a] Jia-Jun Tang,[b] Jia-Hui Ye,[c] Hong Ji[a] and Dan-Lin Yan *[a]

Received 16th August 2022
Accepted 24th October 2022

DOI: 10.1039/d2ra05114a

rsc.li/rsc-advances

Ferroelectric oxides with large bandgaps have restricted applications in photovoltaic and photocatalytic fields. Based on recent experiments with the ferroelectric compound, $LiSbO_3$, the stability and optoelectronic properties of a new ferroelectric compound, namely Li_2SbBiO_6, are investigated in this study. The calculated results demonstrate that Li_2SbBiO_6 satisfies the stability conditions of the elastic coefficients and phonon dynamics. Li_2SbBiO_6 maintains the ferroelectric polarization strength of $LiSbO_3$ and significantly reduces the bandgap, and thus has been explored for applications in photovoltaic and photocatalytic fields. Li_2SbBiO_6 is a new potential ferroelectric oxide for harvesting visible light owing to its suitable bandgap and a large hole–electron effective mass ratio.

1. Introduction

Polar materials with non-centrosymmetric structures have pyroelectric, piezoelectric, ferroelectric, and nonlinear optical properties and have been found to exhibit unique applications in diverse fields.[1–4] The conventional ferroelectric materials, $LiNbO_3$ and $LiTaO_3$, belong to the noncentrosymmetric *R3c* space group and show excellent ferroelectricity and unique features in the photovoltaic and photocatalytic decomposition of water.[5–7] $LiNbO_3$ and $LiTaO_3$ are difficult to be promoted in photovoltaic and photocatalytic applications owing to their wide bandgaps. Some rare-earth ferroelectric oxides such as $LuMnO_3$, $YMnO_3$, and $TbMnO_3$ do not have very strong ferroelectric polarization strengths as $LiNbO_3$ and $BiFeO_3$, but they exhibit excellent band gaps and high absorption coefficients, leading to significant interest in the ferroelectric photovoltaic field.[8,9] The ferroelectric photovoltaic material, $BiFeO_3$, can effectively maintain a high ferroelectric polarization strength and reduce the bandgap by doping to achieve high photovoltaic performance.[10] The bandgap values of ferroelectric oxides with an $LiNbO_3$ structure are usually larger than 3 eV and poorly absorb visible light.[11–15] $LiSbO_3$ with the $LiNbO_3$ structure recently synthesized by Inaguma *et al.* showed potential ferroelectricity and a high ferroelectric Curie temperature.[16] Rich structural phase transitions can appear in $LiSbO_3$ at different pressures with large static dielectric tensor and insulating properties.[17] $LiSbO_3$ with a *R3c* structure has a large bandgap and mainly absorbs ultraviolet light according to our recent study.[18] $LiBiO_3$ with the *Pccn* space group can be prepared *via* the hydrothermal treatment method.[19] Young *et al.* theoretically predicted that the energy of $LiBiO_3$ with a *R3c* structure is relatively close to that of the *Pccn* space group and is a potentially stable ferroelectric photovoltaic material with a strong bulk photovoltaic effect.[20] Bi-based materials have attracted attention for splitting water to produce hydrogen under visible light.[21,22] In Bi-based compounds such as $BiFeO_3$, $BiVO_4$, Bi_2O_3, $KBiO_3$, $LiBiO_3$, and $NaBiO_3$ excited by visible light, the bandgap can be reduced to below 3.0 eV due to hybridization between the O 2p and Bi 6s orbitals.[23,24] The overlapping of O 2p and Bi 6s orbitals in Bi-based photocatalysts is beneficial for decreasing the bandgap to capture visible light.[25] The introduction of Cr ions into $BiFeO_3$ to form the Bi_2FeCrO_6 double perovskite with a *R3* structure can also significantly reduce the bandgap and maintain a high ferroelectric polarization strength, effectively improving photovoltaic efficiency.[26] Considering Sb and Bi elements in the VA group and the unique 6s orbital of the Bi element and double perovskite Bi_2FeCrO_6 with the *R3* structure, the introduction of Bi elements to form Li_2SbBiO_6 in the ferroelectric material $LiSbO_3$ can aid ferroelectric materials with the absorption of visible light. In this study, the stability and optoelectronic properties of Li_2SbBiO_6 are investigated using first-principles calculations. The calculation results show that Li_2SbBiO_6 satisfies stability conditions and maintains the ferroelectric

[a]*Department of Physics, School of Science, Guangdong University of Petrochemical Technology, Maoming, Guangdong 525000, PR China. E-mail: chenxingyuan@gdupt.edu.cn; dlyan@gdupt.edu.cn; Fax: +86-668-2923567; Tel: +86-668-2923838*

[b]*School of Physics, South China University of Technology, Guangzhou 510640, PR China*

[c]*SINOPEC Guangzhou Branch, Guangzhou 510726, PR China*

strength of $LiSbO_3$, while significantly reducing the bandgap to absorb visible light.

2. The calculation method and structure

First-principles calculations are based on the plane-wave basis set of the VASP software.[27,28] The generalized gradient approximation and the plane pseudopotential wave method are used to deal with the interactions between electrons and ions.[29] The Perdew–Burke–Ernzerhof (PBE) functional is used as the exchange–correlation function.[30] The cutoff energy is chosen to be 520 eV, and the K-point sample including the Γ point is selected to be $6 \times 6 \times 6$. The lattice parameters and atomic positions are completely relaxed in the calculations. The electron self-consistency accuracy is 10^{-6} eV, and the atomic force is less than 0.01 eV $Å^{-1}$. The Heyd–Scuseria–Ernzerhof (HSE) hybrid functional is employed to calculate the bandgap and complex frequency-dependent dielectric matrix in random phase approximation (RPA) schemes with an $8 \times 8 \times 8$ K-point sample.[31] The elastic constants (C_{ij}) are calculated using the strain–stress method in the VASP package with the $8 \times 8 \times 8$ K-point sample.[32] The standard berry phase method was applied to calculate ferroelectric polarization.[33,34] A $2 \times 2 \times 2$ supercell containing 80 atoms was used to calculate the phonon frequency for Li_2SbBiO_6, and a $4 \times 4 \times 4$ K-point sample was used for this supercell. $LiSbO_3$ exhibits the $R3c$ symmetry based on experimental reports,[16] while Li_2SbBiO_6 shows the $R3$ symmetry by Bi substitution for Sb similar to the Bi_2FeCrO_6 double perovskite, as shown in Fig. 1. The calculated lattice parameters are shown in Table 1, where the lattice parameters of $R3c$-$LiSbO_3$ and $R3c$-$LiBiO_3$ are in good agreement with the experimental[16] and theoretical values,[20] respectively.

Table 1 The calculated lattice parameters (lattice constant and angle α)

	$LiSbO_3$	$LiSbO_3$	$LiBiO_3$	$LiBiO_3$	Li_2SbBiO_6
a (Å)	5.39 (ref. 16)	5.46	5.67 (ref. 20)	5.71	5.60
α (°)	56.4 (ref. 16)	56.6	56 (ref. 20)	56.1	56.3

3. The stability of Li_2SbBiO_6

$R3c$-$LiSbO_3$ has six independent elasticity coefficients, while $R3$-Li_2SbBiO_6 has seven independent elasticity coefficients. The calculated elastic coefficients are shown in Table 2. The elastic coefficients of $LiSbO_3$ satisfy the inequalities of the stability conditions of the $R3c$ structure:[35]

$$C_{11} - C_{12} > 0,$$

$$C_{13}^2 < 0.5 \times C_{33} \times (C_{11} + C_{12}),$$

$$C_{14}^2 < 0.5 \times C_{44} \times (C_{11} - C_{12}),$$

$$C_{44} > 0.$$

The seven independent elastic coefficients of Li_2SbBiO_6 also satisfy the stability conditions of the $R3$ space group:[35]

$$C_{11} > |C_{12}|,$$

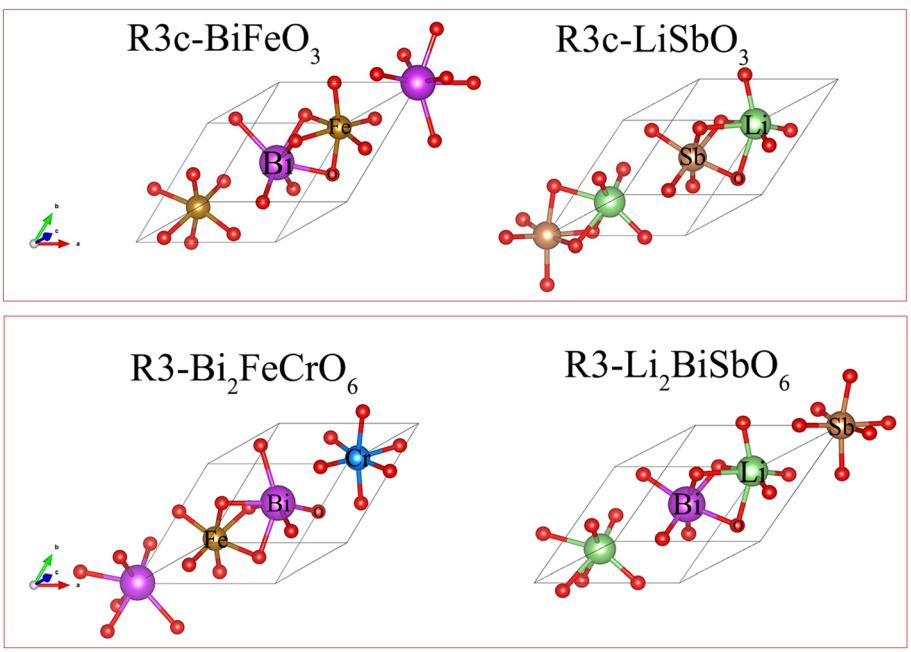

Fig. 1 The structures of $LiSbO_3$ and Li_2SbBiO_6.

Table 2 The calculated elastic coefficients (GPa)

	C_{11}	C_{12}	C_{13}	C_{14}	C_{33}	C_{44}	C_{66}
$LiSbO_3$(present)	245.3	52.0	86.4	−23.4	258.6	112.9	—
$LiSbO_3$ (ref. 18)	283.6	56.2	104.0	−28.8	308.7	135.0	—
$LiSbO_3$(10 GPa) (ref. 18)	322.3	77.8	130.3	−32.2	336.4	150.8	—
$LiSbO_3$(10 GPa) (ref. 17)	289.6	75.0	119.8	−28.5	304.1	135.9	—
$LiSbO_3$(12 GPa) (ref. 17)	295.8	79.3	124.6	−28.9	309.8	138.3	—
Li_2BiSbO_6	196.7	50.2	68.7	−16.2	200.1	84.3	73.2

Table 3 The calculated eigenvalue matrices of elastic coefficients (GPa)

	λ_1	λ_2	λ_3	λ_4	λ_5	λ_6
$LiSbO_3$	79.7	100.7	131.1	156.2	207.6	396.7
Li_2BiSbO_6	61.6	78.3	101.0	124.2	159.1	318.7

$$C_{13}^2 < 0.5 \times C_{33} \times (C_{11} + C_{12}),$$

$$C_{14}^2 + C_{15}^2 < 0.5 \times C_{44} \times (C_{11} - C_{12}),$$

$$C_{44} > 0.$$

The elasticity coefficient of *R*3*c*-$LiSbO_3$ calculated using the PBE function is smaller than that of the SCAN function (Table 2),[18] and the elasticity coefficient becomes larger under high pressure conditions according to reports in the literature.[17,18] All elasticity coefficients of *R*3*c*-$LiSbO_3$ and *R*3-Li_2SbBiO_6 in Table 2 meet the stability conditions. The eigenvalue matrices of the elastic coefficients of $LiSbO_3$ and Li_2SbBiO_6 in Table 3 are greater than 0 and satisfy the mechanical stability condition. The phonon frequencies and phonon density of states were calculated to verify the stability of $LiSbO_3$ and Li_2SbBiO_6 (Fig. 2). The results show that they are potentially stable structures with no imaginary frequencies throughout the Brillouin zone. Li_2SbBiO_6 has a smaller elasticity coefficient than $LiSbO_3$, which implies that mechanical properties, such as Young's modulus, bulk modulus, and hardness, may be modulated by the mutual

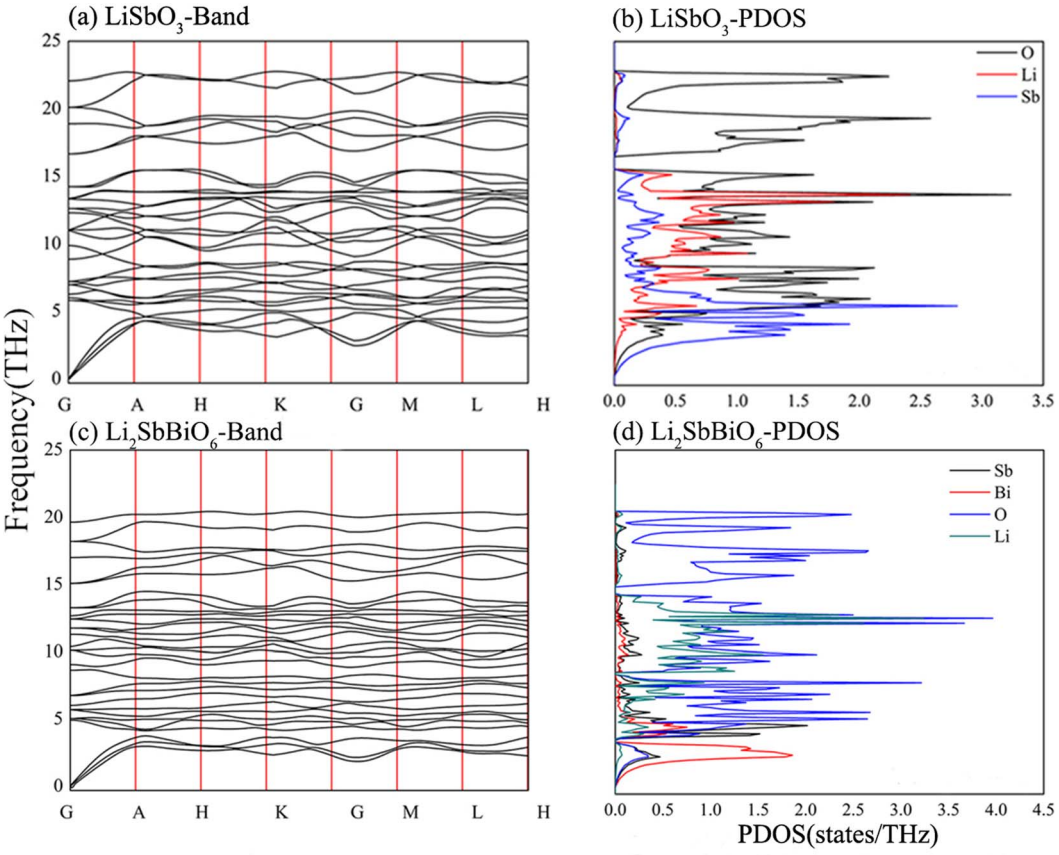

Fig. 2 The calculated phonon frequency and phonon density of states.

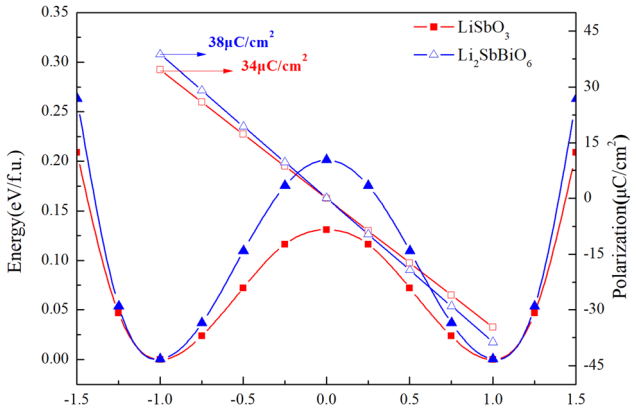

Fig. 3 The calculated energy and polarization as the position of the atom changes.

doping of Sb and Bi. The calculated phonon density of state shows that the phonon frequency of Li_2SbBiO_6 shifts toward lower frequencies as compared to that of $LiSbO_3$, which is in line with the trend of the reduced elasticity coefficient.

4. Ferroelectricity analysis

The ferroelectric polarization strengths of $LiSbO_3$ and Li_2SbBiO_6 are calculated using the berry phase method. As shown in Fig. 3, the energy curves and ferroelectric polarization strengths are calculated by the linear interpolation of the atomic positions between the centrosymmetric and polarized structures. The centrosymmetric and polarized structures for $LiSbO_3$ are $R\bar{3}c$ and $R3c$, respectively, while $R\bar{3}$ and $R3$ structures are chosen for Li_2SbBiO_6. Displacement-type ferroelectric materials can form energy double potential well curves between the ferroelectric (polar) and paraelectric (centrosymmetric) states. The calculated energies of $LiSbO_3$ and Li_2SbBiO_6 show significant ferroelectric double potential wells. Interestingly, the calculated ferroelectric polarization values of $LiSbO_3$ and Li_2SbBiO_6 are 34 μc cm^{-2} and 39 μc cm^{-2}, respectively. Thus, the ferroelectric polarization strength of Li_2SbBiO_6 is slightly greater than that of $LiSbO_3$. According to our previous study, Li–O atomic interactions play a significant role in the ferroelectricity of $LiSbO_3$.[18] We further calculated the effect of the ionic movement on the ferroelectricity of Li_2SbBiO_6 (Fig. 4). The movement of Li–O atoms induces the double potential well shift and promotes the ferroelectric stability in Li_2SbBiO_6. This is consistent with the results of the phonon density of states calculations (Fig. 2), where evidently the Li–O phonon coupling effect is stronger in the high phonon frequency area.

5. Discussion of photoelectric properties

As shown in Fig. 5, $LiSbO_3$ and Li_2SbBiO_6 present the characteristics of an indirect bandgap material with 3.2 and 1.9 eV bandgap values, respectively. The calculated bandgap of $LiSbO_3$ using the HSE06 functional is close to the value (3.4 eV) of the MBJ functional as-obtained in our earlier report.[18] The energy band of Li_2SbBiO_6 has been calculated using the HSE06 + SOC (spin orbit coupling) approach due to the heavy Bi element. The calculation results from Fig. 6 show that the energy band structure of Li_2SbBiO_6 remains basically unchanged by the SOC effect, and the bandgap increases slightly to 2.1 eV. Considering the calculation of HSE06 + SOC is relatively expensive and HSE06 calculations can usually give accurate results in general, the HSE06 approach is mainly used to calculate the optical properties and electronic density of states of Li_2SbBiO_6. The bandgap of Li_2SbBiO_6 maintains the nature of the indirect bandgap of $LiSbO_3$, which is unfavorable for photovoltaic performance, but the introduction of Bi ions can significantly reduce the bandgap to absorb visible light. From the density of states calculations (Fig. 5), the valence charges of both $LiSbO_3$ and Li_2SbBiO_6 mainly comprise O-2p orbitals. It is also found that the antibonding states formed by O-2p and Bi-6s orbitals significantly reduce the bandgap of Li_2SbBiO_6. The absorption coefficients ($\alpha(\omega)$) of Li_2SbBiO_6 were acquired using the frequency-dependent dielectric matrix:

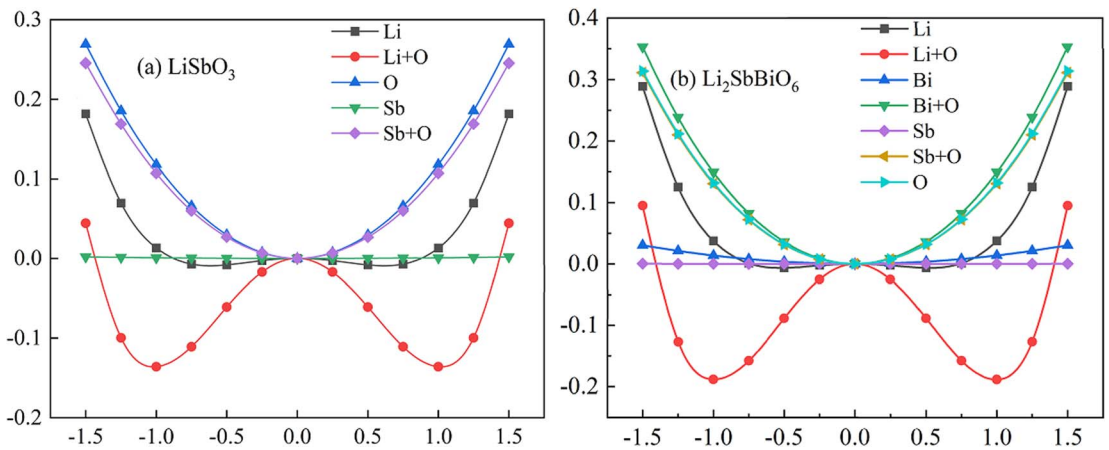

Fig. 4 The calculated energy as the position changes with the movement of different atoms.

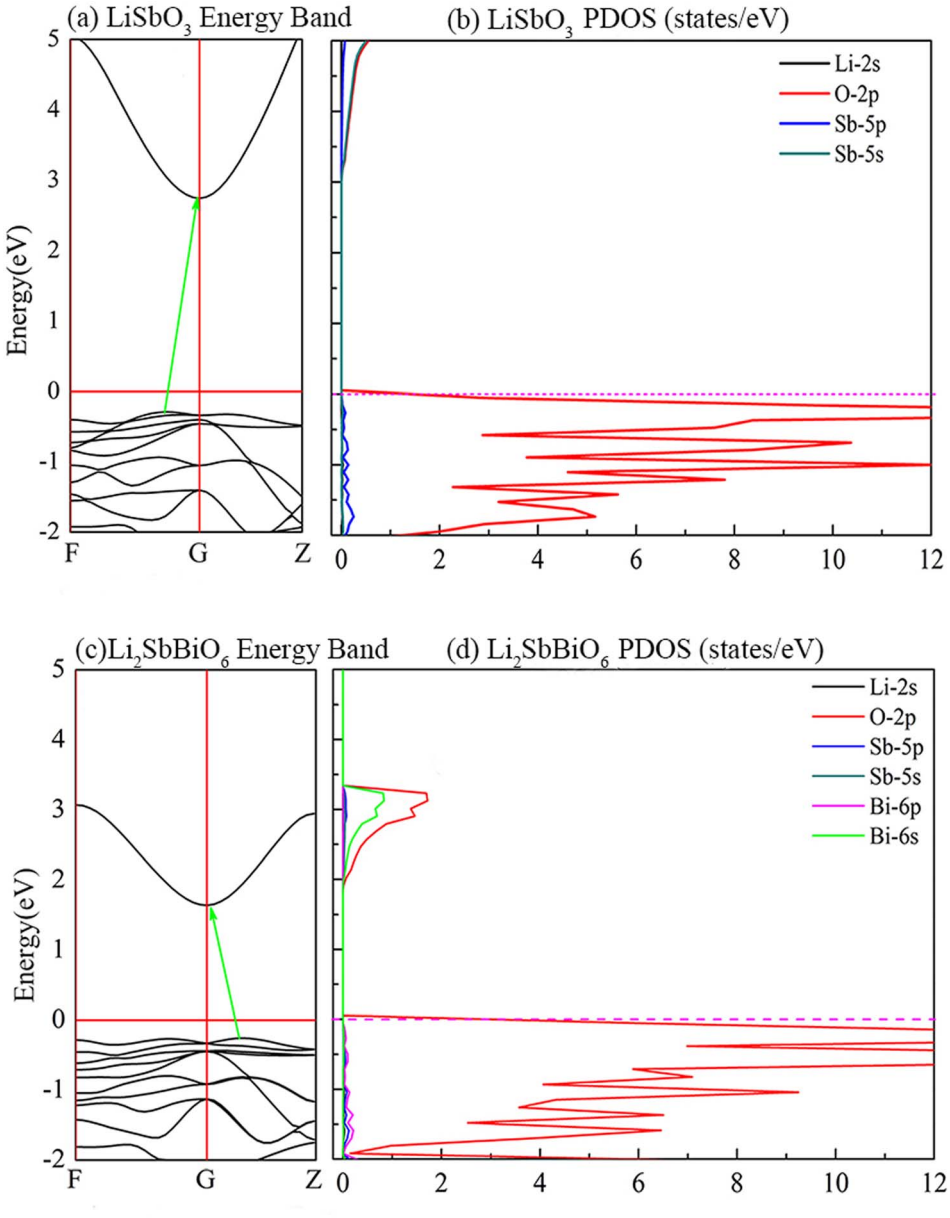

Fig. 5 The calculated energy band structure and density of states.

$$\alpha(\omega) = \frac{2\omega}{c}\left(\frac{\sqrt{\varepsilon_r(\omega)^2 + \varepsilon_i(\omega)^2} - \varepsilon_r(\omega)^2}{2}\right)^{\frac{1}{2}}$$

where ω is the incident light frequency, and c is the speed of light in a vacuum. The imaginary and real parts of the dielectric function are denoted by ε_i and ε_r, respectively. The calculated absorption coefficient of Li_2SbBiO_6 is shown in Fig. 7. $LiSbO_3$ does not absorb visible light because of its large bandgap. Li_2SbBiO_6 can significantly absorb visible light and is a potential ferroelectric photovoltaic material. The bandgap of Li_2SbBiO_6 using the HSE06 calculation is 1.9 eV, which is close to that of the photocatalytic materials BiOI[36] and $LiBiO_3$ (ref. 37) with applications in photocatalytic water splitting. The bandgap value of Li_2SbBiO_6 is not as favorable as that of rare-earth ferroelectric oxides for absorbing visible light,[8,9] but the ferroelectric polarization strength of Li_2SbBiO_6 is relatively large, which could be favorable for driving carrier separation by the depolarization field. A ferroelectric material with an internal electric field can reduce the probability of carrier recombination and improve the efficiency of photogenerated carriers. We calculated the effective mass to investigate the photoelectric properties. The expression for effective mass is $m^*(k) = \pm\hbar^2[\partial^2 E(k)/\partial^2 k]^{-1}$. The calculation results of the effective mass and ferroelectric polarization strength are shown in Table 4. The calculated electron effective mass of $LiSbO_3$ and Li_2SbBiO_6

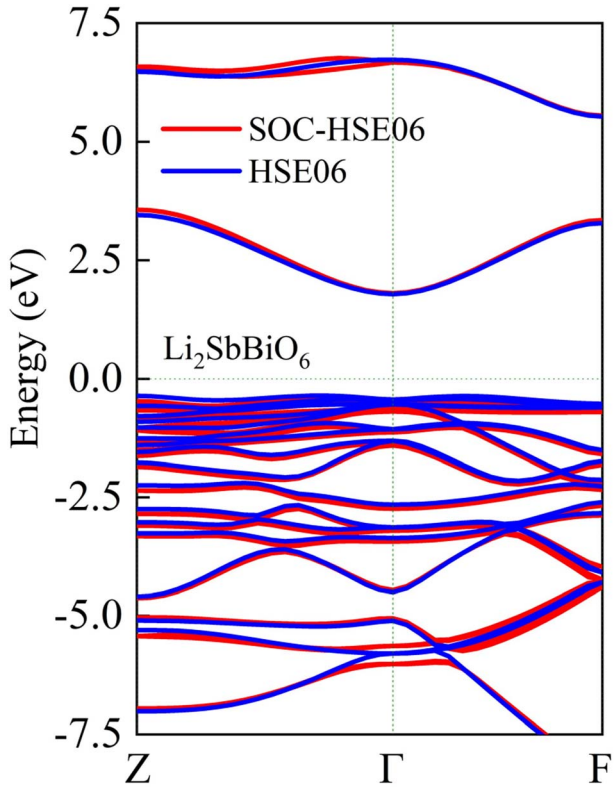

Fig. 6 The calculated energy band of Li_2SbBiO_6 with and without the SOC effect.

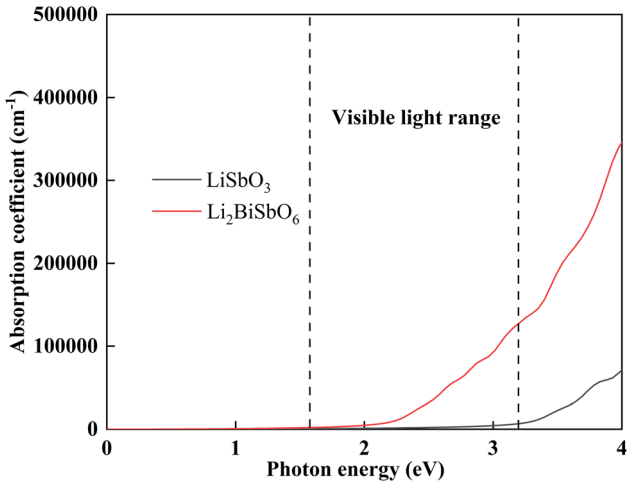

Fig. 7 The calculated light absorption coefficient.

is close to $0.5m_0$, and the electron carrier mobility could be larger due to the small effective mass. The ratio of m_h/m_e was calculated to further explore the response to photoelectric performance. A lower recombination rate and higher transfer rate of photogenerated carriers could be induced for a larger ratio of m_h/m_e. The m_h/m_e ratios of Li_2SbBiO_6 are 7.414 and 5.934 without and with the SOC effect, respectively, which are greater than those of $LiSbO_3$ polarized structures. The m_h/m_e ratio of the ferroelectric material $BiFeO_3$ is 4.589,[38] and the ferroelectric polarization strength is higher than that of Li_2SbBiO_6, but the bandgap of $BiFeO_3$ is relatively large and absorbs only a small amount of visible light for photocatalytic properties.[39,40] The high degradation efficiency could arise from the strong visible light absorption, depolarization field of ferroelectrics, intrinsic small carrier effective mass, and large m_h/m_e ratio in Li_2SbBiO_6, which contribute to the photoinduced carrier separation in the photocatalytic process.

6. Conclusions

The stability and photoelectric properties of the Li_2SbBiO_6 ferroelectric compound have been investigated using density functional theory. The calculation results as well as the elastic coefficient and phonon dynamics analyses show that Li_2SbBiO_6 is a potentially stable ferroelectric material. The ferroelectric stability of Li_2SbBiO_6 and $LiSbO_3$ is related to the strong effect of the Li–O bond. Li_2SbBiO_6 slightly improves the ferroelectric polarization of $LiSbO_3$ and significantly reduces the bandgap to expand its applications in photovoltaic and photocatalysis with visible light. The larger m_h/m_e ratio of Li_2SbBiO_6 accompanied by a suitable bandgap and ferroelectric properties is more favorable for the separation of carriers and absorption of visible light.

Conflicts of interest

The authors declared that they have no conflicts of interest to this work. We declare that we do not have any commercial or associative interest that represents a conflict of interest in connection with the work submitted.

Acknowledgements

This work was supported by the Natural Science Foundation of Guangdong Province, China (Grant No. 2019A1515011914, 2018A030307028, and 2019A1515010916), Maoming Natural Science Foundation of Guangdong, China (Grant No. 2019018001), Guangdong University Student Climbing Project,

Table 4 The calculated effective mass of holes (m_h) and electrons (m_e), the ratio of m_h/m_e, and ferroelectric polarization strength (P_s)

Compounds	m_h (m_0)	m_e (m_0)	m_h/m_e	P_s (μc cm^{-2})
$LiSbO_3$	1.484	0.433	3.424	34
$LiBiO_3$	1.651	0.504	3.272	47 (50 (ref. 20))
Li_2SbBiO_6	3.618(3.258-soc)	0.488(0.549-soc)	7.414(5.934-soc)	39
$BiFeO_3$	3.171 (ref. 38)	0.691 (ref. 38)	4.589	90

China (Grant No. pdjh2021a0331), and Natural Science Foundation of Guangdong University of Petrochemical Technology (no. 2017rc19).

References

1 P. S. Halasyamani and K. R. Poeppelmeier, Noncentrosymmetric oxides, *Chem. Mater.*, 1998, **10**(10), 2753–2769.
2 Y. Zhang, P. T. T. Phuong, E. Roake, *et al.*, Thermal energy harvesting using pyroelectric-electrochemical coupling in ferroelectric materials, *Joule*, 2020, **4**(2), 301–309.
3 C. Wu, G. Yang, M. G. Humphrey, *et al.*, Recent advances in ultraviolet and deep-ultraviolet second-order nonlinear optical crystals, *J. Coord. Chem.*, 2018, **375**, 459–488.
4 Y. Zhang, W. Jie, P. Chen, *et al.*, Ferroelectric and piezoelectric effects on the optical process in advanced materials and devices, *Adv. Mater.*, 2018, **30**(34), 1707007.
5 I. Inbar and R. E. Cohen, Origin of ferroelectricity in $LiNbO_3$ and $LiTaO_3$, *Ferroelectrics*, 1997, **194**(1), 83–95.
6 A. M. Glass, D. Linde and T. J. Negran, High-voltage bulk photovoltaic effect and the photorefractive process in $LiNbO_3$[M], *Landmark Papers On Photorefractive Nonlinear Optics*, 1995, pp. 371–373.
7 S. Takasugi, K. Tomita, M. Iwaoka, *et al.*, The hydrothermal and solvothermal synthesis of $LiTaO_3$ photocatalyst: Suppressing the deterioration of the water splitting activity without using a cocatalyst, *Int. J. Hydrogen Energy*, 2015, **40**(16), 5638–5643.
8 H. Han, S. Song, J. H. Lee, *et al.*, Switchable photovoltaic effects in hexagonal manganite thin films having narrow band gaps, *Chem. Mater.*, 2015, **27**(21), 7425–7432.
9 X. Huang, T. R. Paudel, S. Dong, *et al.*, Hexagonal rare-earth manganites as promising photovoltaics and light polarizers, *Phys. Rev. B: Condens. Matter Mater. Phys.*, 2015, **92**(12), 125201.
10 L. You, F. Zheng, L. Fang, *et al.*, Enhancing ferroelectric photovoltaic effect by polar order engineering, *Sci. Adv.*, 2018, **4**(7), 3438.
11 J. He, C. Franchini and J. M. Rondinelli, Lithium niobate-type oxides as visible light photovoltaic materials, *Chem. Mater*, 2016, **28**(1), 25–29.
12 K. P. Ong, X. Fan, A. Subedi, *et al.*, Transparent conducting properties of $SrSnO_3$ and $ZnSnO_3$, *APL Mater.*, 2015, **3**(6), 062505.
13 J. Zhang, B. Xu, Y. S. Wang, *et al.*, First-principles investigation of the ferroelectric, piezoelectric and nonlinear optical properties of $LiNbO_3$-type $ZnTiO_3$, *Sci. Rep.*, 2019, **9**(1), 1–14.
14 X. F. Xu, X. L. Cai, K. R. Su, *et al.*, Tuning mechanical properties, ferroelectric properties and electronic structure in *R3c*-$MgSnO_3$ by compressive strain: A first-principle study, *Phys. B*, 2021, 413143.
15 K. Fujiwara, H. Minato, J. Shiogai, *et al.*, Thin-film stabilization of $LiNbO_3$-type $ZnSnO_3$ and $MgSnO_3$ by molecular-beam epitaxy, *APL Mater.*, 2019, **7**(2), 022505.
16 Y. Inaguma, A. Aimi, D. Mori, *et al.*, High-pressure synthesis, crystal structure, chemical bonding, and ferroelectricity of $LiNbO_3$-type $LiSbO_3$, *Inorg. Chem.*, 2018, **57**(24), 15462–15473.
17 S. M. Yang, A. J. Mao, H. Cheng, *et al.*, Pressure-Induced High-κ Dielectric Properties and Multiple Phase Transitions between Novel Nonperovskite and Perovskite Phases in $LiSbO_3$: A First-Principles Study, *J. Phys. Chem. C*, 2020, **125**(1), 878–885.
18 K. R. Su, X. F. Xu, G. X. Lai, *et al.*, First-principles investigation of the elastic, photocatalytic and ferroelectric properties of $LiNbO_3$-type $LiSbO_3$ under high pressure, *Mater. Today Commun.*, 2021, **27**, 102406.
19 T. Takei, R. Haramoto, Q. Dong, *et al.*, Photocatalytic activities of various pentavalent bismuthates under visible light irradiation, *J. Solid State Chem.*, 2011, **184**(8), 2017–2022.
20 S. M. Young, F. Zheng and A. M. Rappe, First-Principles Materials Design of High-Performing Bulk Photovoltaics with the $LiNbO_3$ Structure, *Phys. Rev. Appl.*, 2015, **4**(5), 054004.
21 H. Cheng, B. Huang and Y. Dai, Engineering BiOX (X= Cl, Br, I) nanostructures for highly efficient photocatalytic applications, *Nanoscale*, 2014, **6**(4), 2009–2026.
22 S. Y. Yu, L. Zhang, L. B. Zhu, *et al.*, Bismuth-containing semiconductors for photoelectrochemical sensing and biosensing, *Coordin. Chem. Rev*, 2019, **393**, 9–20.
23 S. Cao, P. Zhou and J. Yu, Recent advances in visible light Bi-based photocatalysts, *Chin. J. Catal.*, 2014, **35**(7), 989–1007.
24 R. He, D. Xu, B. Cheng, *et al.*, Review on nanoscale Bi-based photocatalysts, *Nanoscale Horiz.*, 2018, **3**(5), 464–504.
25 M. Xu, J. Yang, C. Sun, *et al.*, Performance enhancement strategies of Bi-based photocatalysts: a review on recent progress, *Chem. Eng. J.*, 2020, **389**, 124402.
26 S. Li, B. AlOtaibi, W. Huang, *et al.*, Epitaxial Bi_2FeCrO_6 multiferroic thin film as a new visible light absorbing photocathode material, *Small*, 2015, **11**(32), 4018–4026.
27 G. Kresse and J. Hafner, *Ab initio* molecular dynamics for liquid metals, *Phys. Rev. B: Condens. Matter Mater. Phys.*, 1993, **47**(1), 558.
28 G. Kresse and J. Furthmüller, Efficient iterative schemes for *ab initio* total-energy calculations using a plane-wave basis set, *Phys. Rev. B: Condens. Matter Mater. Phys.*, 1996, **54**(16), 11169.
29 G. Kresse and D. Joubert, From ultrasoft pseudopotentials to the projector augmented-wave method, *Phys. Rev. B: Condens. Matter Mater. Phys.*, 1999, **59**(3), 1758.
30 J. P. Perdew, K. Burke and M. Ernzerhof, Generalized gradient approximation made simple, *Phys. Rev. Lett.*, 1996, **77**(18), 3865.
31 J. Heyd, G. E. Scuseria and M. Ernzerhof, Hybrid functionals based on a screened Coulomb potential, *J. Chem. Phys.*, 2003, **118**(18), 8207–8215.
32 Y. Le Page and P. Saxe, Symmetry-general least-squares extraction of elastic data for strained materials from *ab initio* calculations of stress, *Phys. Rev. B: Condens. Matter Mater. Phys.*, 2002, **65**(10), 104104.

33 R. D. King-Smith and D. Vanderbilt, Theory of polarization of crystalline solids, *Phys. Rev. B: Condens. Matter Mater. Phys.*, 1993, **47**(3), 1651.
34 N. A. Benedek, A. T. Mulder and C. J. Fennie, Polar octahedral rotations: a path to new multifunctional materials, *J. Solid State Chem.*, 2012, **195**, 11–20.
35 F. Mouhat and F. X. Coudert, Necessary and sufficient elastic stability conditions in various crystal systems, *Phys. Rev. B: Condens. Matter Mater. Phys.*, 2014, **90**(22), 224104.
36 X. Zhang, Z. Ai, F. Jia, *et al.*, Generalized one-pot synthesis, characterization, and photocatalytic activity of hierarchical BiOX (X = Cl, Br, I) nanoplate microspheres, *J. Phys. Chem. C*, 2008, **112**(3), 747–753.
37 R. Ramachandran, M. Sathiya, K. Ramesha, *et al.*, Photocatalytic properties of $KBiO_3$ and $LiBiO_3$ with tunnel structures, *J. Chem. Sci*, 2011, **123**(4), 517–524.
38 J. He, C. Franchini and J. M. Rondinelli, Ferroelectric oxides with strong visible-light absorption from charge ordering, *Chem. Mater.*, 2017, **29**(6), 2445–2451.
39 F. Gao, X. Y. Chen, K. B. Yin, *et al.*, Visible-light photocatalytic properties of weak magnetic $BiFeO_3$ nanoparticles, *Adv. Mater.*, 2007, **19**(19), 2889–2892.
40 S. M. Lam, J. C. Sin and A. R. Mohamed, A newly emerging visible light-responsive $BiFeO_3$ perovskite for photocatalytic applications: a mini review, *Mater. Res. Bull.*, 2017, **90**, 15–30.